Self-rotation of resonant elliptically polarized light in collision-free rubidium vapor

S. M. Rochester[a], D. S. Hsiung[b], D. Budker[a,c,*], R. Y. Chiao[a], D. F. Kimball[a], and V. V. Yashchuk[a]
[a] *Department of Physics, University of California, Berkeley, CA 94720-7300*
[b] *Department of Electrical Engineering and Computer Science, University of California, Berkeley, CA 94720*
[c] *Nuclear Science Division, Lawrence Berkeley National Laboratory, Berkeley CA 94720*
(May 21, 2001)

Self-rotation (SR) of elliptically polarized light resonant with atoms in a collision-free vapor is investigated experimentally and theoretically. Results of density matrix calculations are compared to measurements of SR on the Rb $D1$ and $D2$ lines. It is noted that SR effects involving individual hyperfine transitions are suppressed due to Doppler broadening, and so previously unrecognized effects arising from the interaction of light with multiple hyperfine transitions can become dominant.

PACS. 42.50.Gy, 42.50.Hz, 32.80.Bx

I. INTRODUCTION

Interaction with an elliptically polarized light field can cause an initially isotropic medium to become dichroic and birefringent. The resultant circular birefringence and linear dichroism induce rotation of the polarization ellipse of the light. In the present work, we investigate this effect, known as self-rotation (SR), occurring in a rubidium vapor in which the effect of collisions can be neglected. The vapor is subject to narrow-band cw light near-resonant with the Rb $D1$ (795 nm, ${}^2S_{\frac{1}{2}} \rightarrow {}^2P_{\frac{1}{2}}$) and $D2$ (780 nm, ${}^2S_{\frac{1}{2}} \rightarrow {}^2P_{\frac{3}{2}}$) transitions. Under these conditions, as we discuss below, the previously unrecognized effects of hyperfine structure on SR become important.

Self-rotation provides a convenient experimental method for the measurement of Kerr nonlinearities (see, e.g., Refs. [1,2]) useful for future work on photon-photon interactions and "photon condensed matter" in atomic media [3]. Self-rotation can also be a systematic effect in optical rotation measurements, and is thus important in work employing optical rotation for magnetometry [4,5] and tests of discrete symmetry violations (see, e.g., Refs. [6–9] and references therein). Recently, it has been noted [10] that systems displaying SR can be used for generation of light with non-classical statistical properties, in particular "squeezed vacuum" states. This has been experimentally demonstrated in optical fibers [11]. Resonant atomic vapors could offer significant advantages over optical fibers for producing squeezed states of light due to enhanced optical nonlinearities [12]. The study of SR is also closely related to work on the application of atomic coherences (produced by a strong, resonant light field) to control the polarization state of a relatively weak probe light field [13].

Self-rotation was first observed in molecular liquids [14], where the effect was determined to arise from alignment of anisotropic molecules [15] and electronic polarization of the medium induced by the light field [16]. Self-rotation in resonant atomic vapors, also caused by induced polarization of the medium, has been studied since the late 1960's. The original interest in SR in atomic vapors was related to understanding the polarization of gas laser emission [17]. Later, SR was theoretically examined [18–21] in the context of high-resolution polarization spectroscopy [22]. The theory of SR has also been studied in relation to nonlinear magneto-optical rotation [23,24] and searches for optical rotation due to atomic parity nonconservation [25]. In Refs. [26,27], SR was experimentally studied in the vicinity of Rb resonance lines with broad-band pulsed dye laser radiation. In Ref. [28], SR was studied with a narrow-band cw laser on the potassium $D1$ line. Helium buffer gas was used to broaden the transition, so that the effects of hyperfine structure could be neglected. It was observed that in this system, SR at high light power could not be described in terms of the third-order nonlinear susceptibility, due to saturation effects. Optical pumping was found to be an important mechanism causing SR in a resonant vapor.

Until now, however, the effects of hyperfine structure on SR have not been studied. Under the conditions of the present experiment, those of narrow band laser light and collision-free vapor, we show that effects involving single transitions are suppressed relative to those involving multiple hyperfine transitions. Indeed, the understanding of hyperfine related effects is crucial for the interpretation of the line shapes and magnitudes of SR observed in this experiment. We identify several physical mechanisms that can produce SR: optical pumping, ac Stark shifts, and ac-Stark induced quantum beats, of which optical pumping has been previously discussed, but only in the context of spectrally isolated atomic transitions. The study of SR under the conditions of this experiment is particularly important for applications such as magnetometry [4,5], producing squeezed states of light [12], the study of nonlinear optics at low light levels, and tests of discrete symmetry violations [6–8].

In Sec. II we discuss the roles of optical pumping, ac Stark shifts, and Zeeman coherences in producing SR. We see that for sufficient light power, the effect of both optically pumped orientation as well as ac Stark shift-induced quantum beats (the coherence effect) are im-

portant contributors to SR. In Sec. V, we compare the results of the experiment (discussed in Sec. IV) to the results of a density matrix calculation that incorporates the Rb hyperfine structure (discussed in Sec. III).

II. SELF-ROTATION MECHANISMS

A. Optical pumping

Consider a Doppler-free atomic transition of frequency ω_0 that is spectrally isolated (i.e. the interaction of light with other transitions can be neglected). There are two SR effects (discussed in this and the next subsection) that can be produced in the simplest case of a $J_g = 1/2 \rightarrow J_e = 1/2$ transition, where J_g and J_e are the angular momenta of the lower and upper levels, respectively. Optical pumping by narrow-band elliptically polarized light of frequency ω polarizes the initially isotropic lower level. In order to elucidate the mechanisms responsible for SR we will assume throughout this section that the amplitude E_0 of the optical electric field is small, i.e. that the resonant optical pumping saturation parameter $\kappa = (d^2 E_0^2)/(\hbar^2 \gamma_0 \gamma_t) \ll 1$. Here d is the dipole matrix element, γ_0 is the homogeneous width of the transition, in our case of a collision-free vapor equal to the spontaneous relaxation rate of the upper level, and γ_t is the transit rate of atoms through the light beam (assumed to be much less than γ_0). We choose $\kappa \ll 1$ so that the effects can be treated in the perturbative regime. We also assume that the angle of ellipticity of the light polarization ϵ (equal to the arctangent of the ratio of the minor and major axes of the polarization ellipse [29]) is small. In this case the difference between the populations of the two lower level Zeeman sublevels is $\sim \epsilon\kappa L(\omega)$ times the total lower level population, where $L(\omega)$ is the imaginary part (and $D(\omega)$ is the real part) of the Lorentzian line shape function,

$$D(\omega) + iL(\omega) = \frac{\gamma_0}{2(\omega - \omega_0) + i\gamma_0}, \tag{1}$$

normalized to unity amplitude on resonance. The population difference between the two lower level sublevels causes the magnitude of the real part of the linear susceptibility $\chi_+(\omega)$ for left-circularly polarized (σ_+) light to differ from $\chi_-(\omega)$, that for right-circularly polarized (σ_-) light. This difference induces a phase shift between the σ_+ and σ_- components of the light as it propagates through the medium, which is observed as a change of the angle α of the major axis of the polarization ellipse (Fig. 1). The rotation $\Delta\alpha$ due to this optical pumping effect is

$$\begin{aligned}\Delta\alpha_{op}(\omega) &\approx [\chi_+(\omega) - \chi_-(\omega)]\frac{\pi\omega_0 l}{c} \\ &\approx [\epsilon\kappa L(\omega)][\chi_0 D(\omega)]\frac{\pi\omega_0 l}{c} \\ &\approx \epsilon\kappa\frac{l}{l_0}L(\omega)D(\omega),\end{aligned} \tag{2}$$

where $\chi_0 D(\omega)$ is the real part of the linear susceptibility of the unperturbed medium (we assume $\chi_0 \ll 1$), l is the path length, $l_0 \approx (4\pi\chi_0\omega/c)^{-1}$ is the unsaturated absorption length, and c is the speed of light. The maximum of the rotation with respect to frequency is

$$\Delta\alpha_{\rm op}^{\rm max} \approx \epsilon\kappa\frac{l}{l_0}. \tag{3}$$

B. Ac Stark shifts

For the case of the $1/2 \rightarrow 1/2$ transition, the ac Stark shifts induced by the elliptically polarized light cause a relative shift proportional to ϵ times the scalar shift [30]

$$\delta_{ac}^{\rm scalar}(\omega) \approx \frac{d^2 E_0^2}{\hbar^2\gamma_0}D(\omega) = \kappa\gamma_t D(\omega) \tag{4}$$

between the transition frequencies for σ_+ and σ_- light. The resulting difference between $\chi_+(\omega)$ and $\chi_-(\omega)$ also causes rotation of the polarization ellipse (Fig. 2), proportional to the shift $\sim \epsilon\delta_{ac}^{\rm scalar}(\omega)$ times the slope of the unperturbed susceptibility with respect to frequency:

$$\begin{aligned}\Delta\alpha_{\rm Stark}(\omega) &\approx \epsilon\delta_{ac}^{\rm scalar}(\omega)\frac{d\chi(\omega)}{d\omega}\frac{\pi\omega_0 l}{c} \\ &\approx [\epsilon\kappa\gamma_t D(\omega)][\chi_0\frac{d}{d\omega}D(\omega)]\frac{\pi\omega_0 l}{c} \\ &\approx \epsilon\kappa\gamma_t\frac{l}{l_0}D(\omega)\frac{d}{d\omega}D(\omega).\end{aligned} \tag{5}$$

The maximum rotation is

$$\Delta\alpha_{\rm Stark}^{\rm max} \approx \epsilon\kappa\frac{\gamma_t}{\gamma_0}\frac{l}{l_0}, \tag{6}$$

reduced by a factor of $\sim \gamma_t/\gamma_0$ compared to SR due to the optical pumping effect. This effect is relatively unimportant in our experiment, where $\gamma_t/\gamma_0 \approx 6 \times 10^{-3}$.

C. General isolated $J_g \rightarrow J_e$ transitions

Now consider spectrally isolated $J_g \rightarrow J_e$ transitions with arbitrary angular momenta. In general, these systems will exhibit SR due to both the optical pumping and ac Stark shift effects, except for certain low-J cases: $0 \rightarrow 1$, $1 \rightarrow 0$, and $1 \rightarrow 1$ transitions [17,18,21] (Fig. 3.a–c). In the "dressed atom" approach (which considers the combined atom plus light field system [31]), eigenstates of energy can be either dependent on or independent of light power and detuning. In our case, if the eigenstates are independent of light power and detuning, the projections of these states on the atomic basis are "dark states,"

otherwise, they are "bright states," which do depend on these parameters. Atoms in a dark state are not affected by and do not affect the light field. For a system consisting of a $0 \rightarrow 1$ or $1 \rightarrow 0$ transition and light of arbitrary polarization, there exists only one upper level and one lower level bright state. Since the unperturbed system is optically isotropic, and the only effect of optical pumping is to depopulate the lower bright state, no SR due to optical pumping can occur in such a system. The ac Stark shifts produced by the optical electric field cause shifts of the bright states with respect to the dark states. Thus there is also no SR for $0 \rightarrow 1$ and $1 \rightarrow 0$ transitions by the ac Stark shift mechanism discussed in Sec. II B.

In the absence of repopulation of the lower level due to spontaneous decay from the upper level, a $1 \rightarrow 1$ transition can be decomposed into uncoupled Λ and V subsystems. Neither the Λ nor V subsystem transition exhibits SR, for the same reasons that neither $1 \rightarrow 0$ nor $0 \rightarrow 1$ transitions exhibit SR. Thus $1 \rightarrow 1$ transitions produce no SR. As can be verified by calculation, this conclusion remains unaltered even when spontaneous decay from the upper level repopulates the lower level. It is interesting to note that a $3/2 \rightarrow 1/2$ transition (Fig. 3.d), which can be decomposed into two uncoupled Λ systems, does exhibit SR due to both the optical pumping and ac Stark shift effects. This is because each of the unperturbed Λ subsystems possess intrinsic circular birefringence and dichroism (in the unperturbed system, each of the Λ subsystems induces SR of equal magnitude and opposite sign, so no net optical rotation arises).

D. Ac Stark shift-induced quantum beats

In $J_g \rightarrow J_e$ systems with $J_g > 1/2$ (again, except for $1 \rightarrow 0$ and $1 \rightarrow 1$), SR can also be brought about by quantum beats (evolution of atomic polarization) induced by the optical electric field. This evolution creates alignment (via orientation-to-alignment [32] conversion) not along an axis of light polarization, causing optical rotation due to linear dichroism. (For transitions with $J_g \leq 1/2$, no alignment can be created in the lower level, since it can not possess a quadrupole moment.) This effect is similar to the coherence effects in nonlinear magneto- and electro-optics, which can be thought of as three stage processes (see, e.g., Ref. [4] and references therein) consisting of optical pumping (which produces atomic polarization), quantum beats (which modify atomic polarization), and modification of the polarization of weak probe light as it propagates through the medium (thus probing atomic polarization). In our case, where the lower level relaxation time $\sim 1/\gamma_t$ is much longer than the upper level relaxation time $\sim 1/\gamma_0$, effects due to coherences in the lower level are of primary interest.

Quantum beats occur when there is coherence between lower level components of non-degenerate energy eigenstates. Resonant light polarizes the lower level by pumping atoms out of the bright states. However, in the absence of additional external fields, the bright states are eigenstates of energy. Thus no coherences are created between lower level components of non-degenerate energy eigenstates by depopulation of the lower level alone. Spontaneous decay from the optically excited upper level, on the other hand, can produce coherences (proportional to ϵ when, as throughout this paper, $\epsilon \ll 1$) between non-degenerate eigenstates of elliptically polarized light. For example, in the case of the $1 \rightarrow 2$ transition, a calculation shows that the projections of the energy eigenstates onto the lower atomic level are given by

$$\begin{aligned} \psi_a &= \frac{1+5\epsilon}{\sqrt{2}}|-1\rangle + \frac{1-5\epsilon}{\sqrt{2}}|1\rangle \\ \psi_b &= \frac{-1+5\epsilon}{\sqrt{2}}|-1\rangle + \frac{1+5\epsilon}{\sqrt{2}}|1\rangle \\ \psi_c &= |0\rangle, \end{aligned} \tag{7}$$

where $|m\rangle$ are the Zeeman sublevels with angular momentum projection m in the direction of light propagation ($\hat{z}$). In Fig. 4, surfaces are plotted representing the probability distribution of angular momentum [33] for each of these states; the radius in a given direction is equal to the probability of finding the maximum projection of angular momentum along that direction. During optical pumping, spontaneous emission creates coherence between states ψ_a and ψ_b, which initially corresponds to orientation along $\hat{z}$. The subsequent evolution of the phase of the coherence (Stark-induced quantum beats) produces a component of alignment with an axis at 45° to the major axis of light polarization (Fig. 5). This causes rotation of the polarization of the light as the light propagates through the medium (Fig. 6). This rotation depends on the amount of optically pumped orientation, the size of the tensor Stark shifts $\delta_{ac}^{\text{tensor}}(\omega) \propto \kappa\gamma_t D(\omega)$, the precession time, and the probe frequency:

$$\begin{aligned} \Delta\alpha_{\text{coherence}}(\omega) &\propto [\epsilon\kappa L(\omega)]\left[\frac{\delta_{ac}^{\text{tensor}}(\omega)}{\gamma_t}\right]\left[L(\omega)\frac{l}{l_0}\right] \\ &\propto \epsilon\kappa^2\frac{l}{l_0}D(\omega)L^2(\omega). \end{aligned} \tag{8}$$

Note that in contrast to the effects discussed above, the coherence effect scales as κ^2 at low powers, and thus only becomes important as κ approaches unity.

E. Self-rotation effects involving multiple transitions

In Rb, each (widely separated) hyperfine component of the ground level can interact with multiple more closely-spaced hyperfine components of the upper level. Self-rotation effects caused by the interaction of light with multiple hyperfine transitions are suppressed relative to

the single-transition case because of the upper-level hyperfine separation. However, as we will see below, these effects can become important when Doppler broadening is taken into account.

Consider a non-isolated transition in which there is an additional atomic level ("the neighboring level") that can be coupled to the lower level via the optical field. In this case, SR due to the above effects can be induced by the coupling of the upper and lower levels ("the main transition") in combination with the coupling of the lower level to the upper neighboring level ("the neighboring transition"). For example, atomic orientation can be produced by optical pumping on the main transition and then can rotate the light polarization (be probed) due to interaction on the neighboring transition. This results in SR described by an equation of the form of Eq. (2) but with $D(\omega)$ replaced by the frequency-independent $D(\Delta_0) \approx \gamma_0/(2\Delta_0)$, where Δ_0 is the separation between neighboring states (Fig. 7). While any of the processes of optical pumping, ac Stark shifting, and probing can occur on either the main or the neighboring transitions, those processes with $L(\omega)$ or $\frac{d}{d\omega}D(\omega)$ dependence will be suppressed by a factor $\sim \gamma_0^2/\Delta_0^2$ when occurring on the neighboring transition and can be neglected compared to the dominant multi-transition optical pumping effect described above (which is only suppressed by γ_0/Δ_0). In addition, the multi-transition version of the ac Stark shift effect involves ac Stark shifts in the lower level induced by the neighboring transition and probed on the main transition (Fig. 8). The most important multi-transition coherence effect in our case is where atomic polarization produced by optical pumping on the main transition undergoes quantum beats due to ac Stark shifts induced by the neighboring transition, and is then probed on the main transition (Fig. 9). Here spontaneous decay is not required to produce coherences between lower level components of non-degenerate energy eigenstates, since these components are different for the main and neighboring transitions. In this case, as in the single-transition case, calculations show that the coherences are proportional to ϵ. Self-rotation due to the multi-transition ac Stark shift and coherence effects is described by formulae of the form of Eq. (6,8), respectively, but with $D(\omega)$ replaced by $D(\Delta_0) \approx \gamma_0/(2\Delta_0)$, as before.

The magnitude of the optical rotation due to these multi-transition effects is suppressed by a factor $\sim \gamma_0/\Delta_0$ compared to the single-transition case. However, when Doppler broadening is taken into account, optical rotation that has an average value of zero with respect to detuning, as produced by the single-transition effects and the multi-transition ac Stark shift effect (Figs. 1,2,6,8) will tend to cancel [20], resulting in a suppression of the rotation due to these effects by a factor $\sim \gamma_0/\Gamma_D$ ($\approx 2 \times 10^{-2}$ in our case), where Γ_D is the Doppler width. The multi-transition optical pumping and coherence effects (Figs. 7,9), on the other hand, have non-zero average rotation and no Doppler suppression. In the Doppler-broadened case, therefore, the maximum value of rotation with respect to frequency produced by the multi-transition optical pumping and coherence effects is $\sim \Gamma_D/\Delta_{HF}$ times that due to the single-transition effects. In our experimental situation ($0.5 < \Gamma_D/\Delta_{HF} < 10$, where Δ_{HF} is the upper level hyperfine splitting) we see that the multi-transition optical pumping and coherence effects are important contributors to SR.

F. Self-rotation due to Bennett structures

For light of sufficient intensity, saturation effects perturb the population of various states of atoms in resonant velocity groups. The peaks (corresponding to increased population) and holes (corresponding to reduced population) in the velocity distribution of atoms in a particular state arising from such a process are known as Bennett structures [34]. Ac Stark shifts due to the neighboring transition can cause sub-Doppler features in $\chi_+(\omega)$ and $\chi_-(\omega)$ corresponding to the Bennett structures to be shifted relative to each other. This can in turn lead to optical rotation. This effect is analogous to Bennett-structure-related effects in nonlinear magneto- and electro-optics [35], to be described in detail in a future paper. Compared to the multi-transition optical pumping and coherence effects, SR related to Bennett structures is suppressed by a factor $\sim \gamma_t/\gamma_0$, so is unimportant in the present situation.

III. DESCRIPTION OF THE DENSITY MATRIX CALCULATION

For the present investigation, computer code has been written to model light-atom interactions for atomic systems with hyperfine structure [36]. In Rb, the ground level hyperfine separation of the $D1$ and $D2$ lines is much larger than the excited level separation. Therefore, we treat separately subsystems each containing a hyperfine component of the ground level and all hyperfine components of the excited level accessible via optical transitions from this ground level component. The total angular momenta of the ground and excited level hyperfine components are labeled F_g, F_e respectively, additional ground and excited level quantum numbers are labeled ξ_g, ξ_e. For each subsystem, a density matrix ρ is formed describing the Zeeman sublevels (with angular momentum projection m along the $\hat{z}$-axis) of the relevant hyperfine components of the ground and excited levels. The time evolution of the density matrix under the action of the light-atom interaction Hamiltonian $H_L = -\vec{E} \cdot \vec{d}$, where $\vec{E}$ is the electric field vector, and $\vec{d}$ is the dipole operator, is given by the Liouville equation (see, e.g., Ref. [37]):

$$\frac{d\rho}{dt} = \frac{1}{i\hbar}[H,\rho] - \frac{1}{2}\{\Gamma,\rho\} + \Lambda, \tag{9}$$

where the square brackets denote the commutator and the curly brackets the anti-commutator, and the total Hamiltonian H is the sum of H_L and the unperturbed Hamiltonian H_0. Γ is the relaxation matrix, which is diagonal in the collision-free approximation,

$$\langle \xi F m|\Gamma|\xi F m\rangle = \gamma_t + \gamma_0\delta(\xi,\xi_e), \tag{10}$$

where γ_t and γ_0 are as in the previous section. $\Lambda = \Lambda^t + \Lambda^{repop}$ is the incoherent pumping term, where the diagonal matrix

$$\langle \xi_g F_g m|\Lambda^t|\xi_g F_g m\rangle = \frac{\gamma_t\rho_0}{(2I+1)(2J_g+1)} \tag{11}$$

describes incoherent ground state pumping [38] from the region outside the laser beam (ρ_0 is the atomic density, I is the nuclear spin, and J_g is the ground level electronic angular momentum) and

$$\begin{aligned}\langle \xi_g F_g m|\Lambda^{repop}|\xi_g F_g m'\rangle = \sum_{F_e}\frac{4\omega_0^3}{3\hbar c^3}\frac{\left(\xi_g F_g\|d\|\xi_e F_e\right)^2}{2F_e+1} \\ \times\sum_{m_e,m_e'}\sum_{q=-1}^{1}\left[\langle F_g,m,1,q|F_e,m_e\rangle\right. \\ \times\langle F_g,m',1,q|F_e,m_e'\rangle \\ \left.\times\,\rho_{\xi_e F_e m_e \xi_e F_e m_e'}\right],\end{aligned} \tag{12}$$

describes repopulation due to spontaneous relaxation from the upper level (see, e.g., Ref. [39]). Here $(\ldots\|d\|\ldots)$ indicates the reduced dipole matrix element, and $\langle\ldots|\ldots\rangle$ are the Clebsch-Gordan coefficients. The electric field vector is written (see, e.g., Ref. [29])

$$\begin{aligned}\vec{E} = \frac{1}{2}\Big[E_0 e^{i\phi}(\cos\alpha\cos\epsilon - i\sin\alpha\sin\epsilon)e^{i(\omega t-kz)} + c.c.\Big]\hat{x} \\ + \frac{1}{2}\Big[E_0 e^{i\phi}(\sin\alpha\cos\epsilon + i\cos\alpha\sin\epsilon)e^{i(\omega t-kz)} + c.c.\Big]\hat{y},\end{aligned} \tag{13}$$

where $k = \omega/c$ is the vacuum wave number, ϕ is the overall phase, and E_0, α, ϵ and ω are as defined in the previous section.

To find the stationary solution of Eq. (9), we remove the explicit time dependence by defining

$$\rho_{\xi F m \xi' F' m'} = \begin{cases} x_{\xi F m \xi' F' m'} e^{i\omega t} & \text{for } \xi = \xi_g \text{ and } \xi' = \xi_e \\ x_{\xi F m \xi' F' m'} e^{-i\omega t} & \text{for } \xi = \xi_e \text{ and } \xi' = \xi_g \\ x_{\xi F m \xi' F' m'} & \text{for } \xi = \xi'. \end{cases} \tag{14}$$

We then set $\frac{dx}{dt} = 0$, dropping terms containing $e^{\pm 2i\omega t}$ corresponding to far off-resonance excitation (the rotating wave approximation). This results in a system of time-independent linear equations that can be solved [40] for the equilibrium density matrix.

Substituting Eq. (13) into the wave equation

$$\left(\frac{\omega^2}{c^2} + \frac{d^2}{dz^2}\right)\vec{E} = -\frac{4\pi}{c^2}\frac{d^2}{dt^2}\vec{P}, \tag{15}$$

where $\vec{P} = Tr(\rho\vec{d})$ is the polarization of the medium, and neglecting terms involving second-order derivatives and products of first-order derivatives (thus assuming that changes in α, ϵ, and ϕ and fractional changes in E_0 are small), gives the rotation per unit distance:

$$\begin{aligned}\frac{d\alpha}{dz} = -\frac{2\pi\omega}{E_0 c}\sec 2\epsilon\left[\cos\alpha(P1\sin\epsilon + P4\cos\epsilon)\right. \\ \left. + \sin\alpha(-P2\cos\epsilon + P3\sin\epsilon)\right],\end{aligned} \tag{16}$$

as well as the absorption, phase shift, and change of ellipticity

$$\begin{aligned}\frac{dE_0}{dz} &= -\frac{2\pi\omega}{c}\left[\sin\alpha(-P1\sin\epsilon + P4\cos\epsilon)\right. \\ &\quad \left. + \cos\alpha(P2\cos\epsilon + P3\sin\epsilon)\right], \\ \frac{d\phi}{dz} &= -\frac{2\pi\omega}{E_0 c}\sec 2\epsilon\left[\cos\alpha(P1\cos\epsilon + P4\sin\epsilon)\right. \\ &\quad \left. + \sin\alpha(-P2\sin\epsilon + P3\cos\epsilon)\right], \\ \frac{d\epsilon}{dz} &= \frac{2\pi\omega}{E_0 c}\left[\sin\alpha(P1\cos\epsilon + P4\sin\epsilon)\right. \\ &\quad \left. + \cos\alpha(P2\sin\epsilon - P3\cos\epsilon)\right],\end{aligned}$$

where we have defined

$$\begin{aligned}\vec{P} = \frac{1}{2}\Big[(P1 - iP2)e^{i(\omega t-kz)} + c.c.\Big]\hat{x} \\ + \frac{1}{2}\Big[(P3 - iP4)e^{i(\omega t-kz)} + c.c.\Big]\hat{y}.\end{aligned} \tag{17}$$

Since velocity-changing collisions in the atomic vapor are negligible during the transit time, we can account for Doppler broadening by convolving these quantities with a Gaussian function of width ~ 306 MHz.

When significant absorption takes place, the change in light intensity and ellipticity as the light passes through the atomic medium is no longer small. This is taken into account by integrating absorption, rotation, and change of ellipticity through a series of thin "slices" of the medium.

IV. EXPERIMENTAL APPARATUS AND PROCEDURE

A schematic diagram of the experimental apparatus is shown in Fig. 10. The beam from an external cavity diode laser system (New Focus Vortex 6017 with central wavelength ~ 795 nm for $D1$, EOSI 2010 with central wavelength ~ 780 nm for $D2$), attenuated with crossed film

polarizers, passes through a prism polarizer and a $\lambda/4$ wave plate aligned to produce a small amount of ellipticity in the beam. The beam then passes through an uncoated cylindrical vapor cell (2.5 cm diam. $\times$ 7.5 cm long) inside two layers of magnetic shielding (CONETIC AA alloy). Residual magnetic fields are less than ~ 0.1 mG in any direction. The cell contains a natural mixture of Rb isotopes (72% ^{85}Rb, 28% ^{87}Rb) and no buffer gas. In order to eliminate effects related to back-reflection of laser light from the cell windows, the cell is tilted slightly with respect to the direction of light propagation. A magnetic coil that can provide a uniform magnetic field along the direction of light propagation is installed inside the inner magnetic shield. The coil is used to obtain Faraday rotation data, useful for determining the effective transit time of atoms through the laser beam. Next, the beam passes through a $\lambda/2$ wave plate and finally is split by a polarizing beam splitter (PBS) whose axis is rotated by $\pi/4$ with respect to the axis of the polarizer; the two resulting beams fall onto photodiodes. This "balanced polarimeter" is sensitive to the polarization ellipse rotation while being insensitive to changes in ellipticity.

The $\lambda/2$ wave plate is adjusted so that the rotation angle is near zero far from the atomic resonance, thus compensating for rotation introduced by the $\lambda/4$ plate (a $\lambda/4$ plate whose axis is rotated by an angle ψ with respect to the input linear polarization introduces ellipticity $\epsilon = \psi$ and an equal amount of rotation). This rotation could also be compensated for by adjusting the axis angle of the PBS. However, the PBS used produces a spurious frequency-dependent background signal, caused by interference effects, which is sensitive to optical alignment of the PBS. Using the $\lambda/2$ plate avoids having to adjust the PBS, allowing subtraction of the background signal.

Self-rotation data are taken by tuning the laser through resonance and recording the signal from the photodiodes. Transmission through the Rb vapor is proportional to the sum of the photodiode signals S_1, S_2, while the rotation angle, in the small angle approximation, is given by

$$\Delta\alpha = \frac{S_1 - S_2}{2(S_1 + S_2)}. \tag{18}$$

Files with positive and negative input ϵ are recorded, and the difference between the files is taken, thus removing the background signal produced by the PBS. Density matrix calculations indicate that this procedure also removes the effect of the residual magnetic field on the SR signal. Faraday rotation of the light beam in the presence of a variable longitudinal magnetic field $B_z \approx -200$ mG to 200 mG is also recorded. At these fields, the Faraday rotation is dominated by the coherence transit effect [35] for which the approximate magnetic field dependence is given by [41]

$$\Delta\alpha_{Faraday} \propto \frac{\frac{2g\mu B_z}{\hbar\gamma_t}}{1 + (\frac{2g\mu B_z}{\hbar\gamma_t})^2}, \tag{19}$$

where g is the Landé factor of the lower level and μ is the Bohr magneton. This data is used to determine the effective transit relaxation rate. The control over laser frequency tuning, magnetic field scans, and data acquisition is accomplished using a personal computer with a plug-in data acquisition board and software written in the $Labview^{TM}$ environment.

V. RESULTS AND DISCUSSION

The transmission spectra and hyperfine structure for the Rb $D1$ and $D2$ lines are shown in Fig. 11. Experimental self-rotation spectra for the $D1$ and $D2$ lines at various laser powers, together with predictions of the density matrix calculation, are shown in Figs. 12 and 13, respectively. The non-uniform transverse power distribution in the laser beam and the distribution of atom transit times are not taken into account in the theory. The effective average transit rate is determined by fits of Faraday rotation data to Eq. (19), which gives a value which approximately corresponds to the measured laser beam diameter. The absolute effective laser intensity is determined by matching theory to experiment, while holding fixed the known relative laser power between data sets. The beam diameter corresponding to this effective intensity is a factor of 2 to 3 smaller than the measured beam diameter. This may be due to the highly non-uniform beam profile. This may also be the cause of the discrepancy between SR theory and experiment, which is most pronounced at high light power. Another possible source of discrepancy between theory and experiment is imperfect subtraction of the frequency-dependent background signal produced by the PBS (discussed in Sec. IV). The effective saturation parameter κ ranges from approximately 1 to 100 in these plots, and can be different for different hyperfine components.

Note that for the $D2$ line, SR is primarily of one sign. Among the effects discussed in Sec. II, the multi-transition versions of the optical pumping effect and the coherence effect are the mechanisms that can produce rotation with this characteristic.

The magnitude of SR on the $D1$ line ($\sim \epsilon/100$) is smaller then that for the $D2$ line ($\sim \epsilon/10$), reflecting the fact that the upper-state hyperfine separation is larger for the $D1$ line.

To further illustrate the importance of the multi-transition hyperfine structure effects, we also performed the calculation assuming that each hyperfine transition was isolated. The contributions of each hyperfine transition to optical rotation were calculated separately, accounting for loss to other hyperfine levels, then summed.

Figure 14 compares experimental data to theoretical predictions in both the complete case, and the isolated transition case. The rotation in the isolated transition case is much smaller in magnitude than in the complete case, the dependence of rotation on laser detuning is considerably different, and the average value of the rotation is zero.

VI. SUMMARY AND CONCLUSIONS

We have analyzed the self-rotation phenomenon on the $D1$ and $D2$ lines of rubidium in a collision-free vapor, and have found that effects due to hyperfine structure play an important role. In addition to optical pumping of orientation, the previously unrecognized mechanism of ac Stark-induced evolution of atomic polarization is an important cause of self-rotation in this case. Experimental measurements of self-rotation are in reasonable agreement with the results of a density matrix calculation. This investigation is important for future work on optical rotation, atom-mediated photon-photon interactions, generation of light with non-classical statistics, and tests of discrete symmetries in atomic systems.

Additional experiments have demonstrated that self-rotation in vapor cells with anti-relaxation coating displays very different characteristics [43], including the rotation angle being enhanced, in the case of the $D1$ line, by approximately an order of magnitude. These differences are related to the preservation of atomic polarization over many thousand wall collisions. Self-rotation in anti-relaxation coated cells will be described in future work.

The authors are grateful to M. Mitchell and A. Matsko for helpful discussions and D. Orlando for assistance with the apparatus. This research has been supported by ONR, grants N00014-97-1-0214 and N00014-99-1-0096 and NSF grant 9722535.

---

* e-mail: budker@socrates.Berkeley.edu

[1] R. W. Boyd, *Nonlinear Optics*, Academic Press, 1992.

[2] Kerr nonlinearities due to atomic coherence produced in a model multi-level system are discussed in H. Schmidt and A. Imamoğlu, Opt. Lett. **21**(23), 1936 (1996).

[3] J. Boyce and R. Y. Chiao, Phys. Rev. A **60**, 4114 (1999).

[4] D. Budker, V. Yashchuk, and M. Zolotorev, Phys. Rev. Lett. **81**, 5788 (1998); D. Budker, D. F. Kimball, S. M. Rochester, and V. V. Yashchuk, Phys. Rev. Lett. **85**, 2088 (2000); D. Budker, D. F. Kimball, S. M. Rochester, V. V. Yashchuk, and M. Zolotorev, Phys. Rev. A **62**, 043403.

[5] V. A. Sautenkov, M. D. Lukin, C. J. Bednar, I. Novikova, E. Mikhailov, M. Fleischhauer, V. L. Velichansky, G. R. Welch, and M. O. Scully, Phys. Rev. A **62**, 023810 (2000); M. Fleischhauer, A. B. Matsko, and M. O. Scully, Phys. Rev. A **62**, 013808 (2000); I. Novikova, A. B. Matsko, V. A. Sautenkov, V. L. Velichansky, G. R. Welch, and M. O. Scully, "Ac-Stark shifts in the nonlinear Faraday effect", to be published.

[6] M.-A. Bouchiat and C. Bouchiat, Rep. Prog. Phys. **60** (11), 1351 (1997).

[7] D. Budker, in *Physics Beyond the Standard Model*, P. Herczeg, C. M. Hoffman, and H. V. Klapdor-Kleingrothaus, eds. (World Scientific, Singapore, 1998) pp. 418-441.

[8] L. R. Hunter, Science **252**, 73 (1991).

[9] V. Yashchuk, D. Budker, and M. Zolotorev, in *Trapped Charged Particles and Fundamental Physics*, D. H. E. Dubin and D. Schneider, eds. AIP conference proceedings 457 (AIP Press, Woodbury NY, 1999), pp. 177-181.

[10] L. Boivin and H. A. Haus, Opt. Lett. **21**, 146 (1996).

[11] M. Margalit, C. X. Yu, E. P. Ippen, and H. A. Haus, Opt. Express **2**, 72 (1998).

[12] A. B. Matsko, *et. al.*, (to be published).

[13] S. Wielandy and A. L. Gaeta, Phys. Rev. Lett. **81**, 3359 (1998); S. Wielandy and A. L. Gaeta, in *Quantum Electronics and Laser Science Conference*, OSA Technical Digest (Optical Society of America, Washington DC, 1999), pp. 258-259.

[14] P. D. Maker, R. W. Terhune, and C. M. Savage, Phys. Rev. Lett. **12**(18), 507 (1964).

[15] R. Y. Chiao and J. Godine, Phys. Rev. **185**, 430 (1969).

[16] R. W. Hellwarth, A. Owyoung, and N. George, Phys. Rev. A **4**, 2342 (1971).

[17] A. I. Alexeev and V. M. Galitskii, Zh. Eksp. Theor. Phys. **57**, 1002 (1969) (Sov. Phys. JETP **30**(3), 548 (1970).

[18] S. Saikan, J. Opt. Soc. Am. **68**(9), 1184 (1978).

[19] G. P. Agrawal, Phys. Rev. A **29**(2), 994 (1984).

[20] G. G. Adonts, D. G. Akopyan, and K. V. Arutunyan, J. Phys. B: At. Mol. Phys. **19**, 4113 (1986).

[21] A. I. Alekseev, Zh. Eksp. Theor. Phys. **94**, 130 (1988) (Sov. Phys. JETP **68**(1), 1370 (1988).

[22] C. Wieman and T. W. Hänsch, Phys. Rev. Lett. **36**, 1170 (1976).

[23] S. Giraud-Cotton, V. P. Kaftandjian, and L. Klein, Phys. Rev. A **32**(4), 2211 (1985).

[24] S. V. Fomichev, J. Phys. B: At. Mol. Phys. **28**, 3763 (1995).

[25] N. L. Kosulin and A. M. Tumaikin, Opt. Commun. **59**(3), 188 (1986).

[26] A. M. Bonch-Bruevich, V. A. Khodovoi, and V. V. Khromov, Opt. Spektrosk. **34**, 195 (1973) (Opt. Spectrosc. **34**(1), 109 (1973)).

[27] S. A. Bakhramov, A. T. Berdikulov, A. M. Koharov, and V. V. Tikhonenko, Phys. Lett. **141**(1,2), 31 (1989); S. A. Bakhramov, M. M. Kakhkhorov, and A. M. Kokhkharov, Opt. Spektrosk. **81**(3), 505 (1996) (Opt. Spectrosc. **81**(3), 459 (1996)).

[28] W. V. Davis, A. L. Gaeta, and R. W. Boyd, Opt. Lett. **17** (18), 1304 (1992).

[29] S. Huard, *Polarization of Light* (John Wiley and Sons, New York, 1997). Note that the angle of ellipticity ϵ and

the polarization angle α are related to the Stokes' parameters P_i by $P_3/P_0 = \sin 2\epsilon$ and $P_2/P_0 = \cos 2\epsilon \sin 2\alpha$.

[30] Under the stated conditions, this formula is a good approximation of the expression obtained from dressed state considerations for a two-level atom in, e.g., C. Cohen-Tannoudji, Metrologia **13**, 161 (1977).

[31] C. Cohen-Tannoudji, J. Dupont-Roc, G. Grynberg, *Atom-Photon Interactions* (John Wiley & Sons, New York, 1992).

[32] Here alignment designates the second (quadrupole) polarization moment, and orientation designates the first (dipole) polarization moment, see E. B. Alexandrov, M. P. Chaika, and G. I. Kvostenko, *Interference of Atomic States* (Springer-Verlag, Berlin, 1993).

[33] S. M. Rochester, D. Budker, "Atomic polarization visualized", submitted for publication. Available at http://phylabs.berkeley.edu/budker.

[34] W.R. Bennett, Phys. Rev. **126**, 580 (1962).

[35] D. Budker, D. J. Orlando, and V. Yashchuk, Am. J. Phys. **67**, (1999).

[36] Our calculations are based on principles similar to those applied in F. Schuller, M. J. D. Macpherson, and D. N. Stacey, Physica C **147**, 321 (1987); F. Schuller, M. J. D. Macpherson, and D. N. Stacey, Opt. Commun. **71**, 61 (1989); M. G. Kozlov, Opt. Spectrosc. (USSR) **67**, 789 (1989); S. V. Fomichev, J. Phys. B **24**, 4695 (1991); K. P. Zetie, R. B. Warrington, M. J. D. Macpherson, D. N. Stacey, and F. Schuller, Opt. Commun. **91**, 210 (1992); F. Schuller, D. N. Stacey, R. B. Warrington, and K. P. Zetie, J. Phys. B **28**, 3783 (1995); G. Nienhuis and F. Schuller, Opt. Commun. **151**, 40 (1998).

[37] S. Stenholm, *Foundations of Laser Spectroscopy* (John Wiley and Sons, New York, 1984).

[38] In this work, a vapor cell with no anti-relaxation coating was used. Thus atomic polarization was destroyed by collisions with the cell wall, and so could be ignored in the pumping term.

[39] S. G. Rautian and A. M. Shalagin, *Kinetic problems of non-linear spectroscopy* (North-Holland, New York, 1991).

[40] The system of equations is solved numerically using code written in *Mathematica*, which calls C-language routines employing *Sparse*, a sparse matrix package by K. S. Kundert and A. Sangiovanni-Vincentelli, University of California, Berkeley, April 1988.

[41] S. I. Kanorsky, A. Weis, J. Wurster, and T. W. Hänsch, Phys. Rev. A **47**(2), 1220 (1993).

[42] A. P. Kazantsev, V. S. Smirnov, A. M. Tumaikin, and I. A. Yagofarov, Opt. Spectrosc. **57**(2), 116 (1984).

[43] D. Budker, R. Y. Chiao, D. S. Hsiung, S. M. Rochester, and V. V. Yashchuk, in *Quantum Electronics and Laser Science Conference*, OSA Technical Digest (Optical Society of America, Washington DC, 2000), pg. 252.

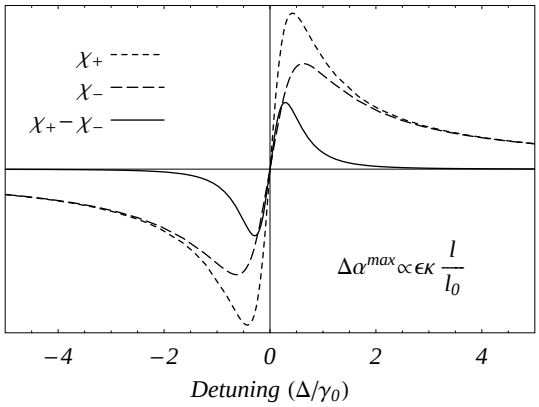

FIG. 1. Spectral dependence of the real parts of the linear susceptibilities $\chi_+(\omega)$ and $\chi_-(\omega)$ for SR due to the optical pumping effect. Differential pumping of σ_+- and σ_--absorbing states produces a difference between $\chi_+(\omega)$ and $\chi_-(\omega)$. The angle of rotation is proportional to this difference.

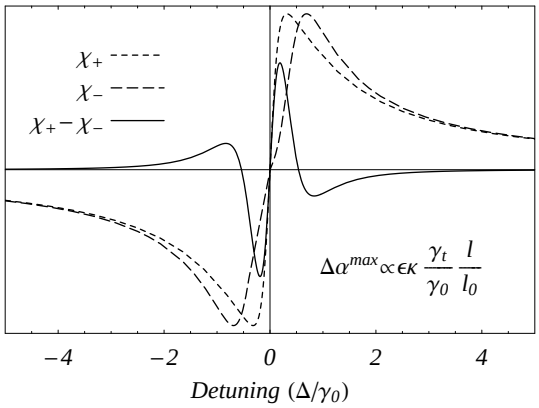

FIG. 2. Spectral dependence of the real parts of the linear susceptibilities $\chi_+(\omega)$ and $\chi_-(\omega)$ for SR due to the resonant ac Stark shift effect. A (frequency dependent) differential Stark shift of the resonance frequencies for σ_+ and σ_- transitions causes a frequency shift between $\chi_+(\omega)$ and $\chi_-(\omega)$. The angle of rotation is proportional to the resulting difference $\chi_+(\omega) - \chi_-(\omega)$.

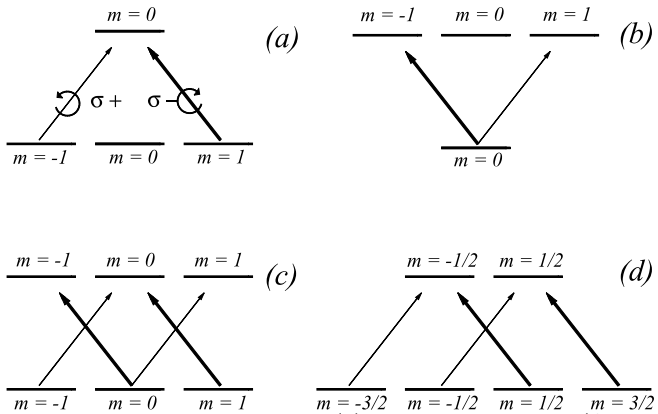

FIG. 3. Level diagrams for (a) a $1 \rightarrow 0$ transition (Λ system), (b) a $0 \rightarrow 1$ transition (V system), (c) a $1 \rightarrow 1$ transition ($\Lambda + \mathrm{V}$ system), (d) a $3/2 \rightarrow 1/2$ transition ($\Lambda + \Lambda$ system).

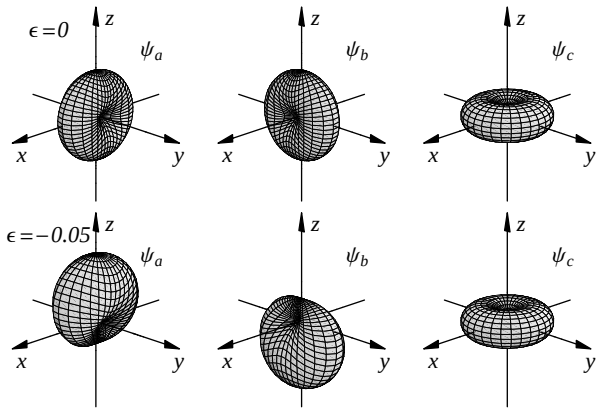

FIG. 4. Probability surfaces (see text and Ref. [33]) corresponding to the lower level components of the energy eigenstates of a $1 \rightarrow 2$ transition interacting with (top row) linearly polarized and (bottom row) elliptically polarized light propagating in the $\hat{z}$-direction.

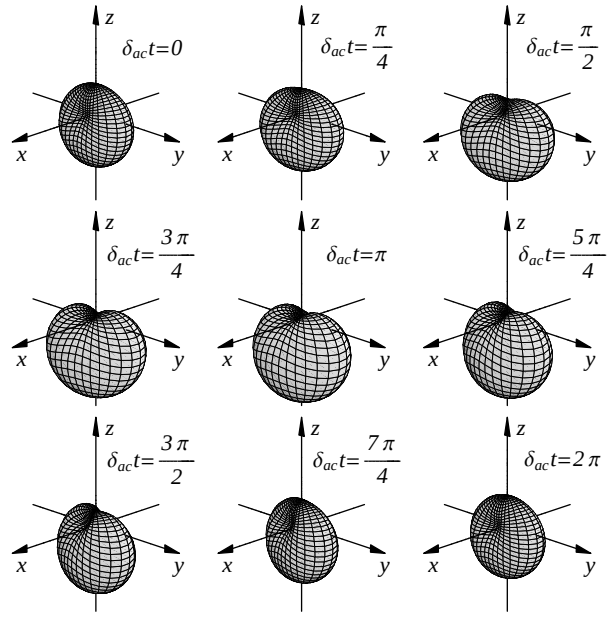

FIG. 5. Evolution (Stark-induced quantum beats) of ground level atomic polarization produced by spontaneous decay from the upper level of a $1 \rightarrow 2$ transition, where δ_{ac} is the tensor Stark shift in the lower level. During the evolution shown above, the elliptically polarized light field ($\epsilon = -0.1$, major axis along x, propagating in the $\hat{z}$ direction) is assumed to be far detuned from resonance so that optical pumping can be neglected. Ground level relaxation is also neglected in this plot.

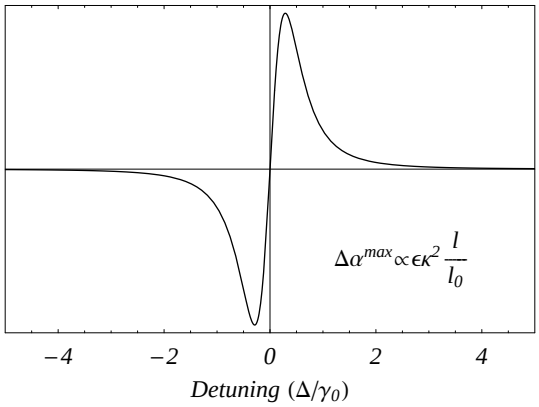

FIG. 6. Spectral dependence of SR due to the coherence effect induced by ac Stark shifts.

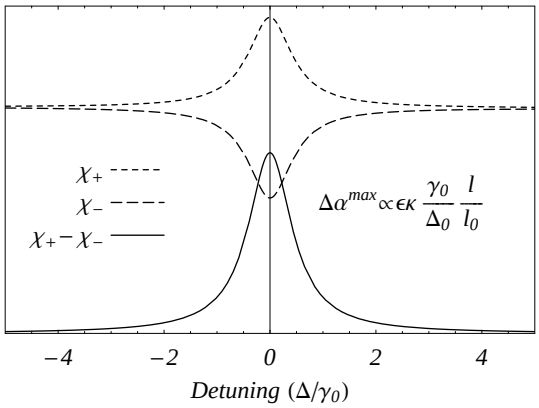

FIG. 7. Spectral dependence of the real parts of the linear susceptibilities $\chi_+(\omega)$ and $\chi_-(\omega)$ for SR due to the multi-transition optical pumping effect. Atomic polarization produced by optical pumping on the main transition causes a difference between $\chi_+(\omega)$ and $\chi_-(\omega)$ when probing on the neighboring transition.

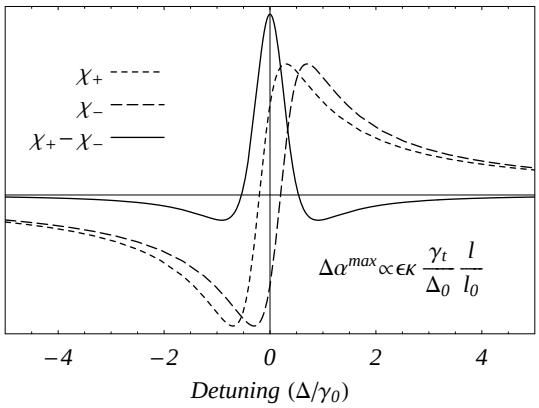

FIG. 8. Spectral dependence of the real parts of the linear susceptibilities $\chi_+(\omega)$ and $\chi_-(\omega)$ for SR due to the multi-transition ac Stark shift effect. A differential Stark shift of the resonance frequencies for σ_+ and σ_- transitions causes a frequency shift between $\chi_+(\omega)$ and $\chi_-(\omega)$. (Detuning is measured relative to the offset line center resulting from the scalar Stark shift.) The resulting optical rotation has a different spectral shape than that of Fig. 2, because the Stark shifts due to the neighboring transition are approximately constant with respect to detuning from the main transition.

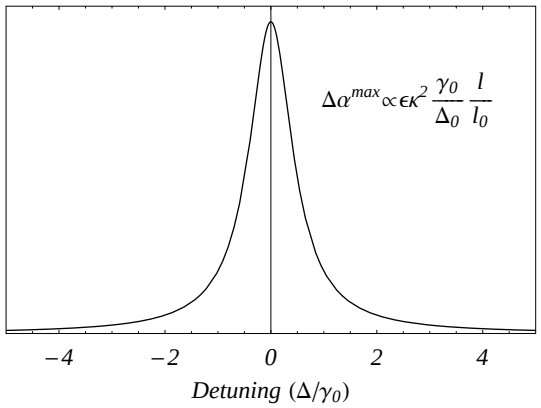

FIG. 9. Spectral dependence of SR due to the multi-transition coherence effect. The atomic polarization evolves in time due to the ac Stark shifts of the lower state induced by the neighboring transition. The resulting optical rotation has a different spectral shape than that of Fig. 6, because the Stark shifts due to the neighboring transition are approximately constant with respect to detuning from the main transition.

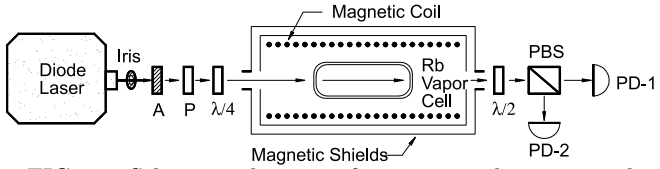

FIG. 10. Schematic diagram of experimental setup, see also Ref. [35]. The laser is an external cavity diode laser. The uncoated cylindrical glass vapor cell contains a natural isotopic mixture of Rb. A – attenuator, P – linear polarizer, PBS – polarizing beamsplitter, PD-1,2 – photodiodes.

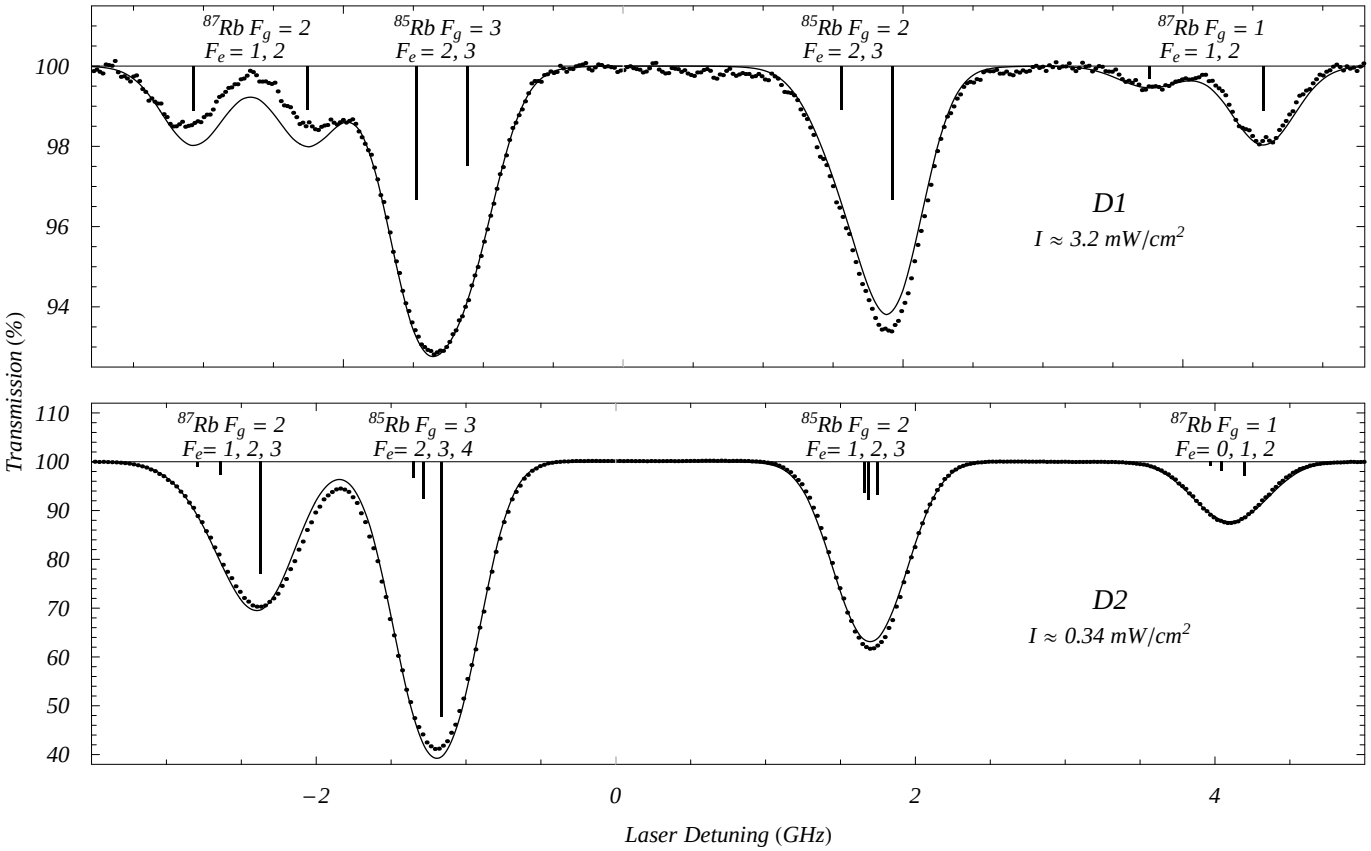

FIG. 11. Experimental data (dots) and theoretical predictions (lines) for transmission on the $D1$ and $D2$ lines of Rb. The vertical bars represent the line strength of the various hyperfine transitions. Theoretical curves were generated from the density matrix calculation with atomic density as a free parameter. The discrepancy between theory and experiment may be due to imperfect correction for interference effects generated by the polarizing beam splitter.

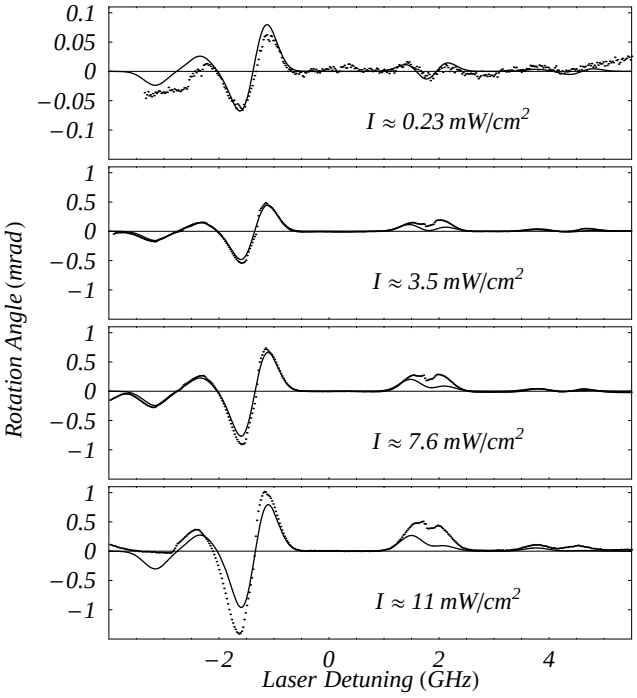

FIG. 12. Data (dots) and theoretical predictions (lines) for SR on the Rb $D1$ line for various laser intensities. The incident angle of ellipticity $\epsilon = 70(8)$ mrad. The atomic density $\sim 8\times10^9$ cm^{-3} is determined from the transmission spectrum. The effective relaxation rate due to atom's transit through the laser beam $\gamma_t \approx 2\pi \times 0.040$ MHz. The laser beam diameter is ~ 3 mm.

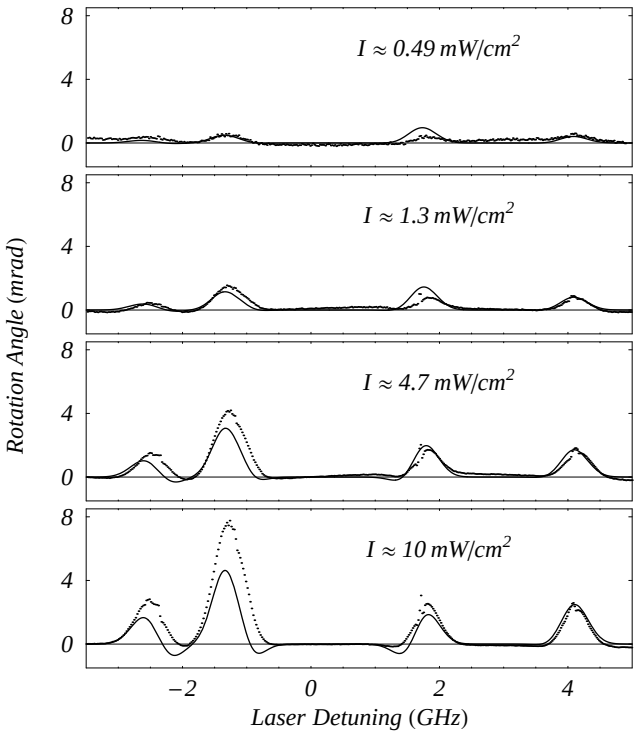

FIG. 13. Data (dots) and theoretical predictions (lines) for SR on the Rb $D2$ line for various laser intensities. The incident angle of ellipticity $\epsilon = 87(8)$ mrad. The atomic density is $\sim 8\times10^9$ cm^{-3}. Effective transit rate is $\gamma_t \approx 2\pi \times 0.073$ MHz. The laser beam diameter is ~ 2 mm.

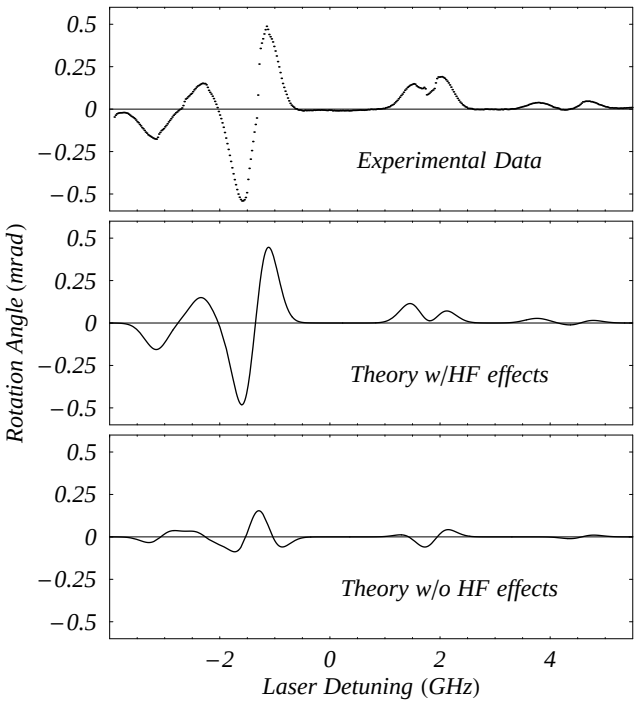

FIG. 14. Comparison of experimental SR data for the Rb $D1$ line, prediction of the theory discussed in Sec. III, and prediction of a theory that treats each hyperfine transition as an isolated transition (see text). Experimental conditions are those described in the caption of Fig. 12, laser intensity $I \approx 3.5$ mW/cm^2.